



# Wear-Resistant Nanostructured Sol-Gel Coatings for Functional Applications

Nadja Felde<sup>1,2,\*</sup>, Luisa Coriand<sup>1</sup>, Angela Duparré<sup>1</sup> and Andreas Tünnermann<sup>1,2</sup>

<sup>1</sup>Fraunhofer Institute for Applied Optics and Precision Engineering, Albert-Einstein-Str. 7, 07745 Jena, Germany

<sup>2</sup>Friedrich-Schiller-University, Institute of Applied Physics, Abbe Center of Photonics, Albert-Einstein-Str. 6, 07745 Jena, Germany

**Abstract:** Improvement of the wear resistance of functional surfaces is crucial in order to facilitate a variety of practical applications, such as self-cleaning or anti-fogging. This especially holds for functional surface nanostructures, whose tops can easily get worn off when exposed to even low abrasion forces. Thus, our work addresses the enhancement of the wear resistance of such fine-scale structures. We present an efficient manufacturing procedure for generating long-term durable surfaces with simultaneously tailored wetting behavior and high optical quality. Our approach is based on a sol-gel coating that consists of an alumina layer with specific nanoroughness yielding the function-relevant surface structure, and a protective thin smooth silica film providing the mechanical robustness without influencing that functional structure. The roughness of the alumina layer can be systematically adjusted, thus enabling us to achieve desired wetting effects all the way up to superhydrophilicity and, after application of an additional thin hydrophobic top coat, to superhydrophobicity. To demonstrate the enhanced robustness of these coatings we perform abrasive wear tests and investigate the impact of abrasion cycles on the wetting effects and optical properties of the coatings. Furthermore, the durability of the structures is directly revealed by advanced roughness characterization procedures based on Atomic Force Microscopy followed by power spectral density function (PSD) analysis.

Received on 10-10-2016  
 Accepted on 11-11-2016  
 Published on 21-12-2016

**Keywords:** Durable thin film coating, Surface roughness, Wetting, Superhydrophobic surface, Superhydrophilic surface, Optical coating, Scatter losses.

DOI: <http://dx.doi.org/10.6000/2369-3355.2016.03.03.1>

## 1. INTRODUCTION

Over the last decades the role of functional surfaces has considerably changed. There is an ongoing trend of requests for surfaces that cover several different functionalities at once [1, 2]. Prominent examples are combinations of extreme wetting behavior, special optical properties, and high mechanical robustness. The technical realization of such multifunctionality enables e.g. equipping optical components with self-cleaning, anti-fogging or anti-icing effects while ensuring long-term stability.

Especially the roughness structure of the surface, in addition to the chemical composition, has been shown to be responsible for such smart wetting behavior [3, 4]. However, the first fundamental basics for this relationship were set by Wenzel as well as Cassie and Baxter [5, 6]. Utilizing these theoretical studies various methods have been developed in the last decades to realize specific wetting properties like

superhydrophobicity [7-9], superhydrophilicity [10, 11] as well as anti-icing behavior [12, 13].

Although surface roughness is required for such functionalities, it can also be a critical factor in regard to optical applications. This is mainly because even small amounts of surface roughness can induce light scattering causing in acceptable optical properties [14, 15]. This problem can however be addressed by shifting the roughness structures to lateral scales that reduce or even prevent scatter losses in the visible range. Since about a decade ago, stochastic nanostructures have therefore become a focus of research as suitable candidates for realizing optical functional surfaces [16-19]. But compared to microscale features, the practical use of such nanorough components remained strongly limited as a result of their poor mechanical robustness. Applying even moderate forces to the surface results in a relatively fast destruction of the structures and simultaneously in a loss of the specific wetting behavior as well as the optical quality. In contrast to a smooth functional layer, which is easily replaceable by simple film deposition techniques (shown exemplarily in [20]), a rough structure is

\*Nadja Felde, Fraunhofer Institute for Applied Optics and Precision Engineering, Albert-Einstein-Str. 7, 07745 Jena, Germany; Tel: +493641 807316; Fax: +493641 807602; E-mail: nadja.felde@iof.fraunhofer.de

not restorable in only one single process step. This results in a high demand on mechanically durable surface roughness structures.

In the last years, however, a large number of reports have been published on durable functional surfaces adopting different manufacturing processes (see e.g. overview in [21]). Various investigations were based on examples from nature like the Lotus Leaf with its hierarchical roughness structure [22]. In addition to microscale or hierarchical wear-resistant roughness structures [23, 24] durable nanostructured surfaces which exhibit high optical quality at the same time have attracted particular interest. In the majority of these studies nanostructures are generated on glass surfaces by phase-separation procedures [25, 26], reactive ion-etching [27] or self-assembly methods [28]. In the light of cost reduction requirements, the sol-gel process is also described as a preferred method [29-32] where the derived structures are mostly formed by nanoparticles. Whereas numerous papers concentrate on superhydrophobic surfaces, the coating in [26] displays both, long-term superhydrophilicity and after applying a hydrophobic top coating also superhydrophobicity with low contact angle hysteresis  $< 3^\circ$ . One main problem in the literature so far is the use of the term “durability” for robustness regarding chemical attack [33, 34], UV radiation [32, 35] or particle contamination. Even if the mechanical stability of rough structures is investigated, an objective assessment of the wear resistance is often hindered by the lack of quantitative determination of the abrasion. The effect of wear remains mostly indirectly estimated by comparative contact angle measurements, e.g. in [25, 28]. Here different weak criteria are used like the change of the apparent water contact angle without any differentiation of the specific wetting system. Even if the structure is investigated, only AFM or SEM images (e.g. in [27, 36]) are demonstrated, relevant roughness properties are not presented or solely by simple roughness parameters as rms-roughness [37]. However, reliable prediction of the long-term stability of a given surface requires a direct estimation of the durability by comprehensive roughness characterization methods.

Thus, as described above, protection of the function-relevant roughness characteristics constitutes an essential

precondition for a successful technical realization of durable surfaces. In our paper we will therefore present an efficient way to manufacture a surface with tailored wetting properties and high optical quality utilizing a sol-gel dip-coating process, where the functional structures are protected against wear. This coating consists of a nanorough alumina layer, responsible for the function-relevant surface roughness and a upper layer of silica, which largely enhances the mechanical durability of the whole system [38]. Well determined roughening of the alumina film roughness enables us to adjust the wettability for both hydrophilicity and – after depositing a hydrophobic top layer – hydrophobicity. In this work, the increased mechanical robustness of the multifunctional coating will be quantified by advanced roughness analysis using power spectral density functions [39].

## 2. EXPERIMENTAL

### 2.1. Nanorough Coating Preparation

Nanorough coatings based on  $\text{Al}_2\text{O}_3$  films were deposited on borosilicate glass substrates (120 mm x 60 mm x 3 mm) using sol-gel and dip-coating processes [40]. The alumina bottom layer was prepared by a standard process using aluminum tri-sec-butoxide, isopropyl alcohol, ethyl acetoacetate, and water [41]. The sol was dip-coated onto the glass substrates and dried afterwards at  $300^\circ\text{C}$ . In order to obtain the derived surface roughness, the smooth  $\text{Al}_2\text{O}_3$  films then underwent post-treatment in distilled boiling water for various periods (0 s to 600 s) and heat-treatment again at  $300^\circ\text{C}$ .

After cooling down, an additional thin smooth  $\text{SiO}_2$  film was applied onto the nanostructure by sol-gel dip-coating to improve the mechanical robustness of the coating. Therefore, a silica sol with a solid content of 5.4 wt% was prepared via hydrolysis and condensation of tetraethylorthosilicat in presence of ethanol, hydrochloric acid, and distilled water. After dip-coating, heat-treatment was carried out at  $300^\circ\text{C}$  for 10 min. The precise adjustment of the dip-coating and heat-treatment processes could be ensured that the initial alumina roughness structure was not negatively affected. For

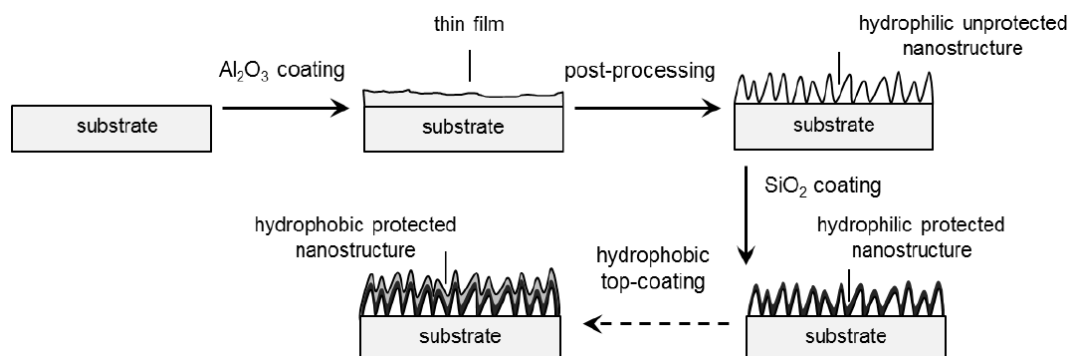


**Figure 1:** Preparation procedure of mechanically durable functional surfaces.

maximum enhancement of the protective function, the silica film thickness was chosen between 40 nm and 50 nm.

Both layer materials, alumina as well as silica, show intrinsic hydrophilic behavior. In order to deliver hydrophobic wetting properties, the surface chemistry of the nanorough samples had to be altered by applying a thin hydrophobic perfluoropolyether top layer (DuralonUltraTec/ COTEC GmbH) using the same dip-coating process. Figure 1 summarizes the entire sample preparation procedure.

## 2.2. Characterization of Surface Structures

Roughness characterization of the samples was performed using Atomic Force Microscopy (AFM; Dimension Icon/ Bruker) in spatial frequency ranges from  $0.1 \mu\text{m}^{-1}$  to  $1000 \mu\text{m}^{-1}$ , corresponding to scan areas from  $50 \times 50 \mu\text{m}^2$  to  $0.2 \times 0.2 \mu\text{m}^2$ . For quantitative roughness analysis, the two-dimensional power spectral density (PSD) function was calculated for each measurement area [39]:

$$PSD(f_x, f_y) = \lim_{L \rightarrow \infty} \frac{1}{L^2} \left| \int_{-\frac{L}{2}}^{\frac{L}{2}} \int_{-\frac{L}{2}}^{\frac{L}{2}} (h(x, y) \cdot e^{-2\pi i(f_x x + f_y y)}) dx dy \right|^2, \quad (1)$$

where  $h(x, y)$  denotes the topographic surface data,  $L$  the scan size, and  $f_x, f_y$  the spatial frequency components. The PSD function (Eq. 1) describes the relative strength of each roughness component as a function of the spatial frequency. Furthermore, it enables a direct link between the roughness characteristics and the wetting behavior of a given stochastic surface. A subsequent data reduction procedure of the PSD function leads to the wetting parameter  $\kappa_B$  [42, 43], which was used in this work to separate the influence of the roughness characteristics and the material properties on the wetting behavior. Previous studies [44, 45] showed that a  $\kappa_B$  value of at least 0.4 is necessary to reach an extreme wetting behavior e.g. superhydrophobicity.

Additional to the roughness analysis by PSD functions, the root mean square (rms) roughness was calculated from the surface topography data. It should be mentioned that these measurements can be influenced by noise as well as by the shape of the AFM probe tip. This significantly occurs in the high spatial frequency range ( $10 \mu\text{m}^{-1}$  to  $1000 \mu\text{m}^{-1}$ ). To appropriately estimate the lateral features these factors should hence be known and minimized by optimized measurement parameters and a calibration of the measurement system with suitable standards [46, 47].

## 2.3. Wetting Characterization

For the wetting analysis of hydrophilic as well as hydrophobic surfaces, an OCA20 measurement system (Data Physics GmbH) was used. Hydrophobic surfaces were investigated by measuring the advancing (ACA) and receding contact angles (RCA), as well as the roll-off angles  $\alpha$ , and the bounce-off angles  $\alpha_{bo}$  [45]. Surfaces with  $ACA \geq 150^\circ$ , low

hysteresis (ACA-RCA) [48], and roll-off angles  $\leq 10^\circ$  were declared as superhydrophobic [45].

For the wetting analysis of hydrophilic samples, however, the ACA and RCA measurements fail as a result of a vanishing RCA. Therefore, the analysis was instead performed by determining the apparent contact angle (CA) as a function of the wetting time  $t$  [45]. Strong hydrophilic behavior with  $CA < 5^\circ$  within a few seconds was referred to as superhydrophilicity.

## 2.4. Light Scattering Measurements

For optical investigations, light scattering measurements were performed using the instrument ALBATROSS-TT (3D-Arrangement for Laser Based Transmittance, Reflectance, and Optical Scatter Measurement-Table Top/ Fraunhofer IOF) [49] at a wavelength  $\lambda$  of 640 nm. Scatter losses were determined as angle resolved scattering (ARS) and total scattering in the transmission hemisphere ( $TS_t$ ) by integration of the ARS data [50].

## 2.5. Mechanical Durability Testing

To investigate the mechanical robustness of the nanorough coatings, abrasive wear measurements were carried out with a Universal Mechanical Tester (UMT-1/ Bruker). Here the samples were wiped in a multiple-slide test against a counter surface ( $2 \text{ cm} \times 2 \text{ cm}$ ) covered with a microfiber lens cleaning tissue applying a normal load of 1.5 N and varied number of wiping cycles (1 to 150). To ensure a controlled mechanical stress to the structures, the following parameters were chosen for the investigations: sliding distance 4 cm and sliding speed 5 mm/s. The results were then evaluated by roughness measurements. Using these data, PSD functions and  $\kappa_B$  values were calculated for quantitative estimation of the durability.

## 3. RESULTS AND DISCUSSION

### 3.1. Adjustable Surface Roughness

Figure 2 presents the nanostructures of five selected samples (alumina coated with silica) compared to the surface of a bare glass substrate. The AFM images and the rms-roughness reveal the systematically graded surface roughness from sample #1 to sample #5 as a consequence of the increased immersion time of the alumina film in boiling water (0 s to 300 s).

This post-treatment step allows the initial smooth  $\text{Al}_2\text{O}_3$  film (cf. sample #1) to react with water resulting in boehmite crystals ( $\text{AlO}(\text{OH})$ ) [41]. As a consequence, the aspect ratio of the surface structure is increasing, clearly exhibited by the corresponding PSD functions (Figure 3). Here the combined PSD functions over the entire measured spatial frequency range are presented. Especially in the high spatial frequency range,  $10 \mu\text{m}^{-1}$  to  $1000 \mu\text{m}^{-1}$ , which is tantamount to lateral

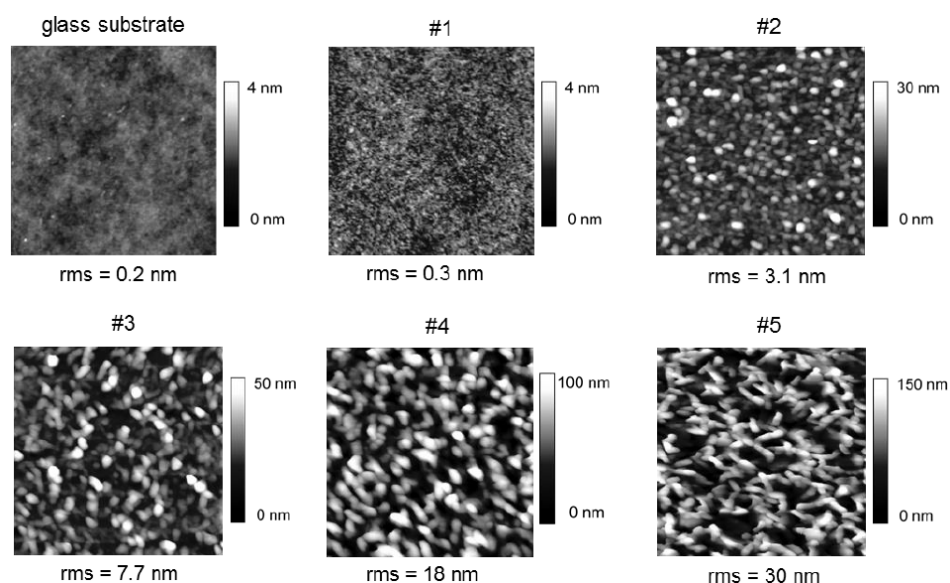


Figure 2: AFM surface topographies (field of view:  $1 \times 1 \mu\text{m}^2$ ) and rms-roughness values of samples #1 to #5 and bare glass substrate.

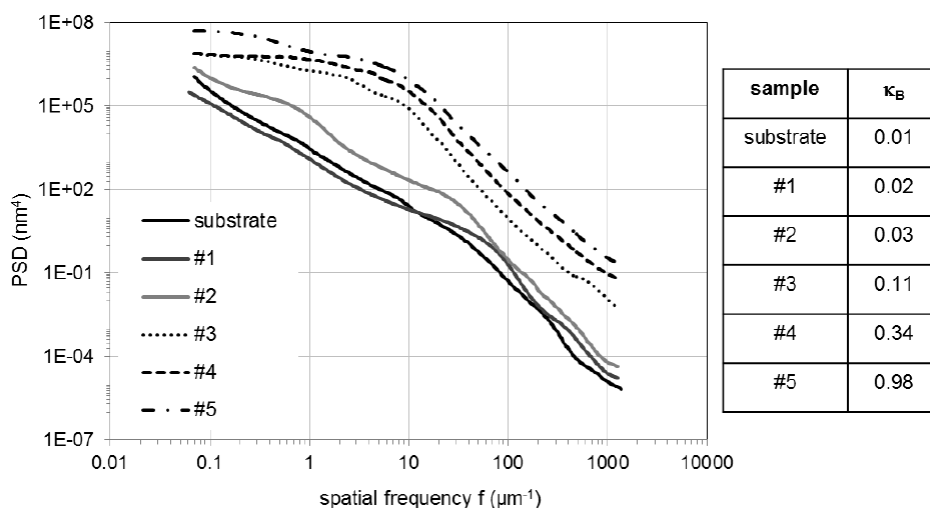


Figure 3: Comparison of PSD functions and  $\kappa_B$  values for sample #1 to sample #5 and bare glass substrate.

components from 100 nm to 1 nm, the PSD values are significantly increasing from sample #1 to sample #5. This spatial frequency range has been shown as to be wetting-relevant for nanorough optical coatings [42]. The derived  $\kappa_B$  values from the PSD data in the spatial frequency range  $0.1 \mu\text{m}^{-1}$  to  $1000 \mu\text{m}^{-1}$ , however, indicate different wetting states of the investigated coatings (see Figure 3). Sample #5 even exceeds the threshold value of 0.4, introduced in section 2.2, and hence open up the potential for extreme wetting behavior, to which is addressed to in the following.

### 3.2. Adjustable Wetting Behavior and Optical Properties

The wetting properties of the nanostructures before and after application of an additional smooth hydrophobic top layer are depicted in Figure 4. The results clearly demonstrate that hydrophobicity and hydrophilicity, respectively, increase with rising surface roughness, all the way up to extreme wetting

behavior. The roughest sample #5 exhibits, in the hydrophilic case, even water CA less than  $5^\circ$ , i.e. complete spreading of water drops within only a few seconds (Figure 5a). The corresponding hydrophobic surface reveals high ACA and RCA of  $155^\circ$  and  $145^\circ$ , respectively, resulting in a hysteresis as low as  $10^\circ$ . This leads water drops with a volume of  $30 \mu\text{l}$  to roll-off at a tilting angle of only  $3^\circ$  and hence confirms the  $\kappa_B$  prediction of possible superhydrophobicity. This means that the surface of sample #5 reaches a sufficiently high aspect ratio of the roughness structure to trap air between the surface and the water drop, also referred to as heterogeneous wetting [6, 51]. In contrast, sample #4 shows comparable ACA values of  $154^\circ$ , but a significant higher CA hysteresis of  $71^\circ$ , indicating a homogeneous wetting state [5]. Although these values do not meet the strict criteria for superhydrophobicity, the sample #4 is still useful for a variety of practical applications due to the bounce-off behavior of

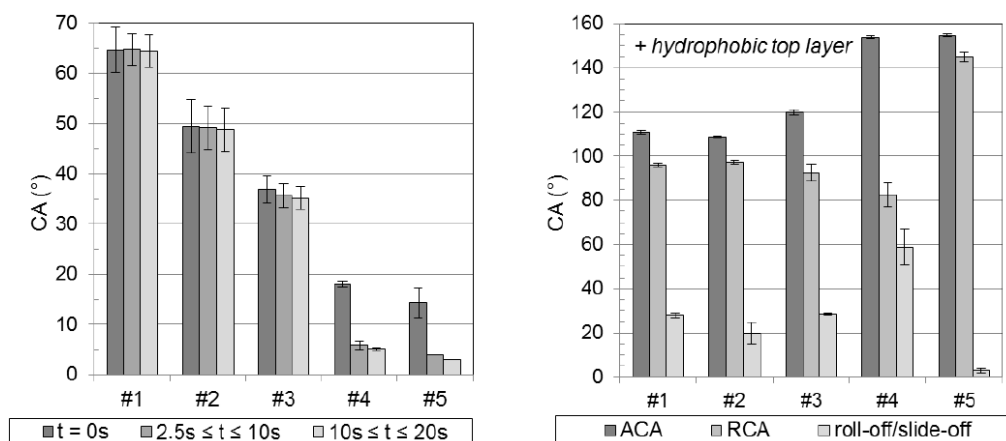


**Figure 4:** CA as a function of the wetting time for hydrophilic coatings #1 to #5 (left); ACA, RCA and roll-off angle for coatings #1 to #5 after applying an additional thin hydrophobic top layer.

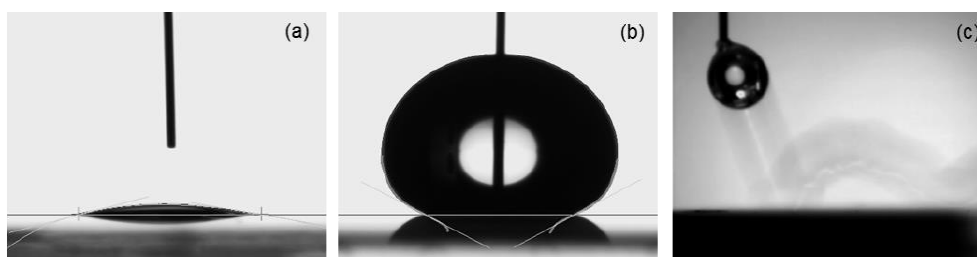


**Figure 5:** (a) Water drop ( $CA = 5^\circ$  at  $t = 2.5$  s) on the superhydrophilic sample #5, (b) water drop ( $ACA = 155^\circ$ ) on the superhydrophobic sample #5, (c) bounce-off test ( $\alpha_{bo} = 20^\circ$ ) on the hydrophobic sample #4.

water drops at low angles of  $20^\circ$  (see section 2.3), as illustrated in Figure 5c.

In addition to the adjustable wetting properties through graded nanoroughness, the presented surfaces show also high transparency with low scatter losses. Compared to the bare glass substrate with scatter losses into the transmission hemisphere amounting to as low as  $TS_f = 0.001\%$ , the roughest sample #5 indicates an insignificant higher value of  $TS_f = 0.007\%$ . As the increased surface roughness, which is related to the more pronounced wetting behavior, predominantly occurs in the high spatial frequency range ( $10 \mu\text{m}^{-1} - 1000 \mu\text{m}^{-1}$ ), it is not negatively affecting the optical quality of the surface in the visible spectral (VIS) region [17].

### 3.4. Enhanced Mechanical Durability

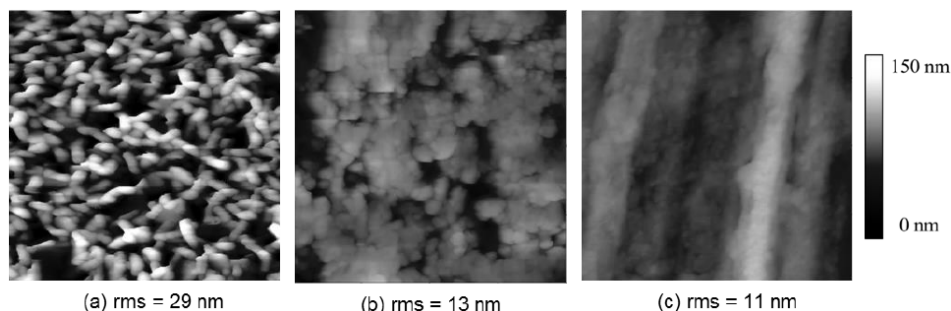
As shown in the previous section, the wetting properties of a surface can be tailored to a large extent by their nanoroughness. However, compared to microscale features, such fine-scale surface structures with high aspect ratios (cf. sample #5) are extremely fragile and can be destroyed by applying even low mechanical stress. This leads to a relatively fast loss of the desired wetting behavior and optical quality. Hence, protection of the rough nanostructures is the most important task in order to transfer such surfaces into practical use.

Regarding the presented coatings, damage of the roughness structure would be most critical for the roughest sample #5.

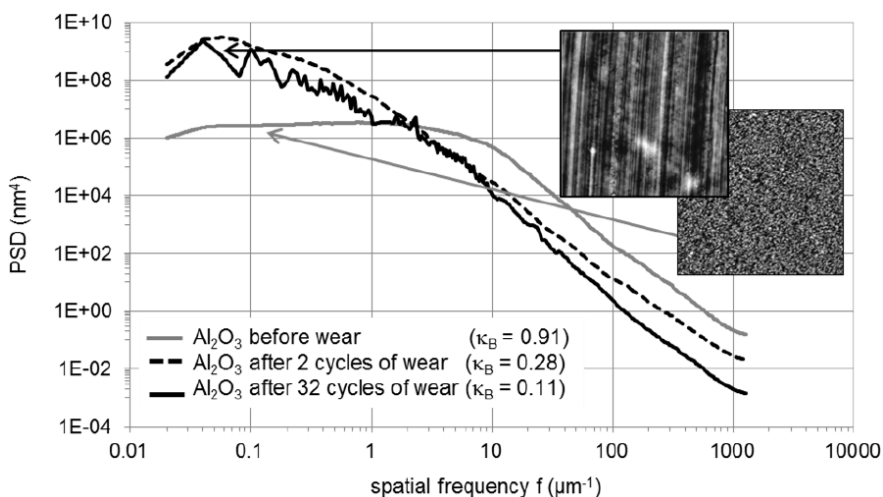
Therefore, in the following the results for abrasion investigations will concentrate on this surface. Further the wear properties of a pure unprotected alumina layer, which exhibits the same roughness characteristics as sample #5, will be demonstrated in the beginning and compared to the properties of sample #5.

Figure 6 illustrates the effects of wear tests with a load of 1.5 N and different wiping cycles on the as introduced pure nanorough alumina layer. The aspect ratio of the nanostructure significantly decreases after only 2 cycles of wear and after 32 wiping cycles a complete damage of the nanostructure is observed.

By analyzing the PSD functions (see Figure 7), the destruction of the nanostructures reveals as a strong decrease of the PSD values in the high spatial frequency range ( $3 \mu\text{m}^{-1}$  to  $1000 \mu\text{m}^{-1}$ ). On the other hand, scratches resulting from the abrasion induce increased PSD values in the spatial frequency range below  $3 \mu\text{m}^{-1}$ . This leads to a significant increase of scattering losses and decrease of the optical quality. By calculating the  $\kappa_B$  values for the surface before and after the applied wear, it can be noticed that there is a decrease from 0.91 to 0.28 after only 2 abrasion cycles, predicting the loss of the extreme wetting behavior. After applying the additional hydrophobic top layer, a significant change of the wetting properties as compared to those before the wear tests occurs, confirming the prediction derived from the roughness analysis. As a consequence of the destroyed



**Figure 6:** AFM topography images (field of view:  $1 \times 1 \mu\text{m}^2$ ) for the unprotected alumina nanostructure (same roughness characteristics as sample #5): (a) before wear, (b) after 2 cycles of wear, (c) after 32 cycles of wear.



**Figure 7:** PSD functions,  $\kappa_B$  values and AFM topography images (field of view:  $10 \times 10 \mu\text{m}^2$ ) for the unprotected alumina nanostructure (same roughness characteristics as sample #5) before and after applied wear.

nanostructure, the wetting regime has changed from the heterogeneous to homogenous causing decreased ACA values of  $134^\circ$  and high roll-off angles of  $31^\circ$ .

A completely different reaction to the applied load, however, was observed when the nanostructures were protected by a thin silica film (cf. sample #5). As compared to the unprotected structure, this surface remains sufficiently intact up to 150 wiping cycles with a force of 1.5 N. After 2 or 32 cycles of abrasion only the tops of the features are slightly modified (see Figure 8), but still maintain the aspect ratio needed for the functional behavior.

More clearly this is presented by the PSD diagram in Figure 9, showing negligible differences between the PSD functions of the protected surface before and after wear with 2 and 32 abrasion cycles. Calculated  $\kappa_B$  values demonstrate that up to 100 abrasion cycles the surface of sample #5 exceeds the  $\kappa_B$  threshold of 0.4 and, hence, shows the potential for superhydrophobicity. Even after 150 abrasion cycles the sample #5 still shows a  $\kappa_B$  value above 0.3.

The contact angles of the samples with the additional thin hydrophobic layer remained nearly unaffected after up to 100 abrasion cycles (see Figure 10b): ACA =  $154^\circ$ , RCA =  $142^\circ$ ,

and  $\alpha = 7^\circ$  i.e. superhydrophobicity was preserved. After further 50 wiping cycles with a force of 1.5 N, the ACA slightly changed to  $141^\circ$ . Although the CA hysteresis increased (see Figure 10c), the sample #5 still shows great bounce-off properties of water, which is sufficient for a wide range of practical applications. Moreover, in the light scattering-relevant spatial frequency range ( $0.05 \mu\text{m}^{-1}$  to  $1.6 \mu\text{m}^{-1}$  for  $\lambda = 640 \text{ nm}$ ) the PSD values are not significantly increasing, which confirms optical quality even after applied wear.

A comparison of the results from roughness and wetting analysis demonstrates that the silica protected nanostructure (sample #5) exhibits a significant higher mechanical durability than the unprotected alumina structure. While alumina as a thin smooth and dense layer is hard and wear resistant, the roughened alumina film exhibits a porous structure with deep valleys and high tips which can easily be abraded. Applying an additional, very thin smooth and hence dense silica layer on top of the rough alumina film protects its roughness structure while completely replicating it. Especially in Figure 9 this improvement is obvious when comparing the PSD function of the unprotected structure after 2 wiping cycles to the PSD function of sample #5 after 150 wiping cycles. Here negligible differences are noticed, stating the same level of

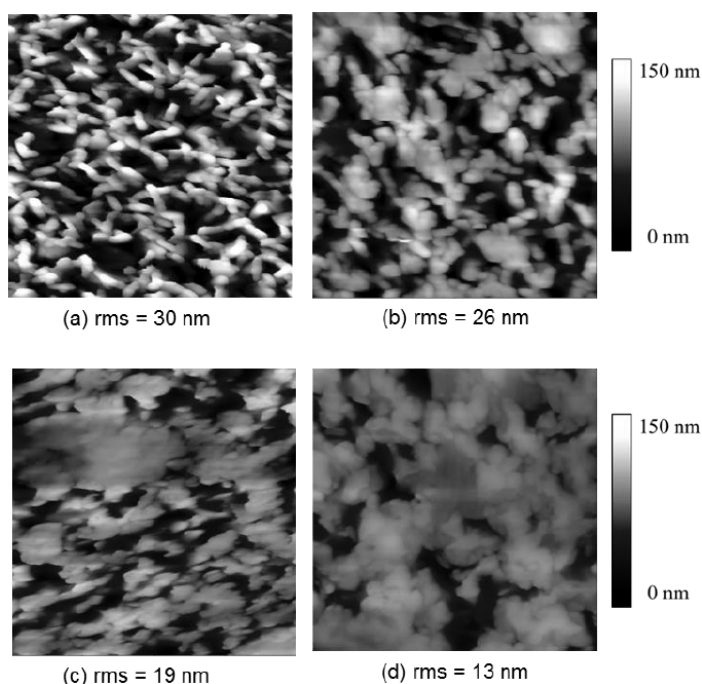


**Figure 8:** AFM topography images (field of view:  $1 \times 1 \mu\text{m}^2$ ) for sample #5: (a) before wear, (b) after 2 cycles of wear, (c) after 32 cycles of wear, (d) after 150 cycles of wear.

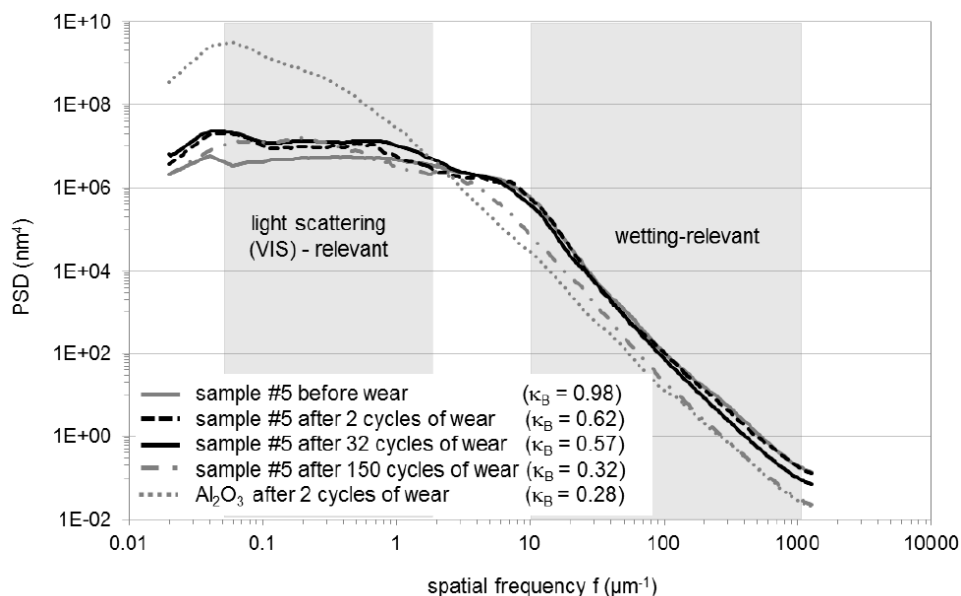


**Figure 9:** PSD functions and  $\kappa_B$  values for sample #5 before and after applied wear. Light scattering ( $\lambda = 640 \text{ nm}$ )- and wetting-relevant spatial frequency ranges are highlighted.

structure abrasion. The findings give therefore a promising approach to apply coatings like that of sample #5 on optical components, where the wear properties are sufficient to ensure long-term use.

#### 4. SUMMARY

The presented study focused on the mechanical durability of nanorough surfaces with enhanced wetting properties. An efficient method has been developed of utilizing a sol-gel dip-

coating process to realize multifunctional coatings on glass surfaces, which combine extreme wetting behavior, optical quality, and high mechanical robustness. The coatings are based on nanorough alumina films with an additional thin silica layer, which does not negatively affect the initial roughness structure. The stochastic surface roughness of the alumina layer was shown to be adjustable by thermal post-treatment. In this way, the desired wetting properties of the coatings were achieved for both hydrophilicity and - after applying an additional thin hydrophobic film - for

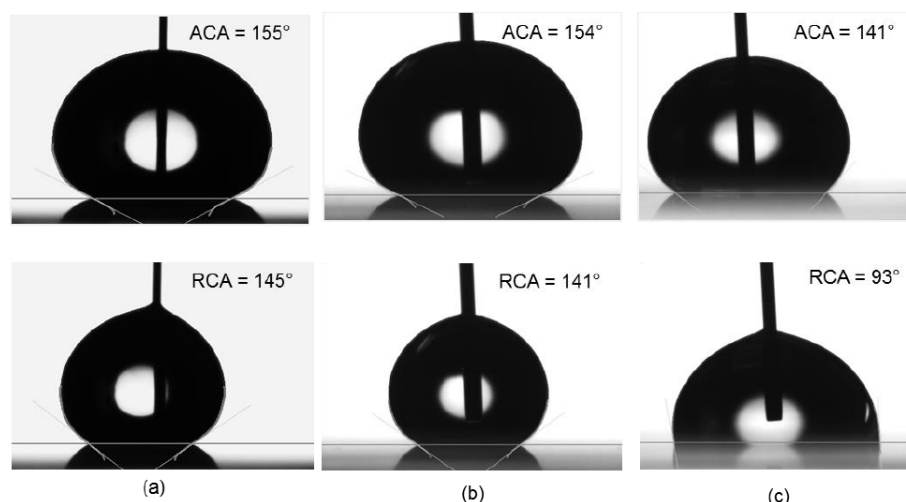


**Figure 10:** Water drop on sample #5 after applying a hydrophobic top layer (a) before applied wear, (b) after 100 cycles of wear, (c) after 150 cycles of wear.

hydrophobicity up to superhydrophobicity. Using specific roughness measurement and analysis procedures enabled us to predict and control the surface roughness for tailoring the wetting properties.

It was demonstrated that the long-term stability of these functional properties as well as the high optical quality significantly depend on the mechanical durability of the surface roughness structures. The combination of the nanorough alumina layer and the protecting silica film, revealed a dramatically improved mechanical wear resistance as compared to surfaces containing alumina structures only. The enhanced mechanical robustness was studied by means of surface roughness analysis using power spectral density functions and a so called wetting parameter that constitutes a reliable indicator for the wetting behavior. The improvement of the wear properties became also evident when the wetting characteristics of the obtained surfaces were controlled after wear. While the alumina nanostructure without the protective layer already lost its superhydrophobic or superhydrophilic properties completely even after application of moderate mechanical stress, the wetting behavior of the protected surfaces was, under the same conditions, preserved till at least 50 times the initial wiping cycles. The fabrication of such nanorough coatings offers hence an effective approach to mechanical durable functional optical surfaces with appropriate reliability in practical applications.

## ACKNOWLEDGEMENTS

The contributions of Alexander v. Finck and Anne-Sophie Munser (Fraunhofer IOF) to the light scattering measurements and fruitful discussions are gratefully acknowledged.

## REFERENCES

- [1] Ragesh P, Anand Ganesh V, Nair SV, Nair AS. A review on self-cleaning and multifunctional materials. *J Mater Chem A* 2014; 2: 14773. <https://doi.org/10.1039/C4TA02542C>

- [2] Cannavale A, Fiorito F, Manca M, Tortorici G, Cingolani R, Gigli G. Multifunctional bioinspired sol-gel coatings for architectural glasses. *Build Environ* 2010; 45: 1233-43. <https://doi.org/10.1016/j.buildenv.2009.11.010>
- [3] Marmur A. Wetting on hydrophobic rough surfaces: to be heterogeneous or not to be? *Langmuir* 2003; 19: 8343-8. <https://doi.org/10.1021/la0344682>
- [4] Quéré D. Rough ideas on wetting. *Phys A Stat Mech its Appl* 2002; 313: 32-46. [https://doi.org/10.1016/S0378-4371\(02\)01033-6](https://doi.org/10.1016/S0378-4371(02)01033-6)
- [5] Wenzel RN. Resistance of solid surfaces to wetting by water. *Ind Eng Chem* 1936; 28: 988-94. <https://doi.org/10.1021/ie50320a024>
- [6] Cassie ABD, Baxter S. Wettability of porous surfaces. *Trans Faraday Soc* 1944; 40: 546. <https://doi.org/10.1039/TF9444000546>
- [7] Fürstner R, Barthlott W, Neinhuis C, Walzel P. Wetting and self-cleaning properties of artificial superhydrophobic surfaces. *Langmuir* 2005; 21: 956-61. <https://doi.org/10.1021/la0401011>
- [8] Koch K, Bhushan B, Jung YC, Barthlott W. Fabrication of artificial Lotus leaves and significance of hierarchical structure for superhydrophobicity and low adhesion. *Soft Matter* 2009; 5: 1386. <https://doi.org/10.1039/b818940d>
- [9] Horowitz F, Brandão LEVS, Camargo KC, Michels AF, Balzaretto NM. Nano-microstructured, superhydrophobic, and infrared transparent polytetrafluoroethylene/diamond films. *J Nanophotonics* 2013; 7: 073596. <https://doi.org/10.1117/1.JNP.7.073596>
- [10] Min Nie, Patel P, Kai Sun, Meng DD. Superhydrophilic anti-fog polyester film by oxygen plasma treatment. In: 2009 4th IEEE International Conference on Nano/Micro Engineered and Molecular Systems IEEE 2009; 1017-20.
- [11] Zhao J, Ma L, Millians W, Wu T, Ming W. Dual-functional antifogging/antimicrobial polymer coating. *ACS Appl Mater Interfaces* 2016; 8: 8737-42. <https://doi.org/10.1021/acsami.6b00748>
- [12] Mazzola L. Aeronautical livery coating with icephobic property. *Surf Eng* 2016; 32: 733-44. <https://doi.org/10.1080/02670844.2015.1121319>
- [13] Kreder MJ, Alvarenga J, Kim P, Aizenberg J. Design of anti-icing surfaces: smooth, textured or slippery? *Nat Rev Mater* 2016; 1: 15003. <https://doi.org/10.1038/natrevmats.2015.3>
- [14] Stover JC. Optical scattering: measurements and analysis, Third Edition Bellingham, Wash. Society of Photo-Optical Instrumentation Engineers; 2012.
- [15] Schröder S, Trost M, Garrick M, et al. Origins of light scattering from thin film coatings. *Thin Solid Films* 2015; 592: 248-55. <https://doi.org/10.1016/j.tsf.2015.02.077>

- [16] Flemming M, Duparré A. Design and characterization of nanostructured ultrahydrophobic coatings. *Appl Opt* 2006; 45: 1397. <https://doi.org/10.1364/AO.45.001397>
- [17] Flemming M, Hultaker A, Reihls K, Duparre A. Modeling and characterizing thin film nanostructures for ultrahydrophobic surfaces with controlled optical scatter. In: Amra C, Kaiser N, Macleod HA, editors. 2004. p. 56.
- [18] Xiu Y, Xiao F, Hess DW, Wong CP. Superhydrophobic optically transparent silica films formed with a eutectic liquid. *Thin Solid Films* 2009; 517: 1610-5. <https://doi.org/10.1016/j.tsf.2008.09.081>
- [19] Su C, Li J, Geng H, Wang Q, Chen Q. Fabrication of an optically transparent super-hydrophobic surface via embedding nano-silica. *Appl Surf Sci* 2006; 253: 2633-6. <https://doi.org/10.1016/j.apsusc.2006.05.038>
- [20] Rangel TC, Michels AF, Horowitz FF, Weibel DE. Superomniphobic and easily repairable coatings on copper substrates based on simple immersion or spray processes. *Langmuir* 2015; 31: 3465-72. <https://doi.org/10.1021/acs.langmuir.5b00193>
- [21] Verho T, Bower C, Andrew P, Franssila S, Ikkala O, Ras RH a. Mechanically durable superhydrophobic surfaces. *Adv Mater* 2011; 23: 673-8. <https://doi.org/10.1002/adma.201003129>
- [22] Barthlott W, Neinhuis C. Purity of the sacred lotus, or escape from contamination in biological surfaces. *Planta* 1997; 202: 1-8. <https://doi.org/10.1007/s004250050096>
- [23] Ebert D, Bhushan B. Durable Lotus-effect surfaces with hierarchical structure using micro- and nanosized hydrophobic silica particles. *J Colloid Interface Sci* 2012; 368: 584-91. <https://doi.org/10.1016/j.jcis.2011.09.049>
- [24] Kondrashov V, Rühle J. Microcones and nanograss: toward mechanically robust superhydrophobic surfaces. *Langmuir* 2014; 30: 4342-50. <https://doi.org/10.1021/la500395e>
- [25] Wang D, Zhang Z, Li Y, Xu C. Highly transparent and durable superhydrophobic hybrid nanoporous coatings fabricated from polysiloxane. *ACS Appl Mater Interfaces* 2014; 6: 10014-21. <https://doi.org/10.1021/am405884x>
- [26] Aytug T, Simpson JT, Lupini AR, *et al.* Optically transparent, mechanically durable, nanostructured superhydrophobic surfaces enabled by spinodally phase-separated glass thin films. *Nanotechnology* 2013; 24: 315602. <https://doi.org/10.1088/0957-4484/24/31/315602>
- [27] Infante D, Koch KW, Mazumder P, *et al.* Durable, superhydrophobic, antireflection, and low haze glass surfaces using scalable metal dewetting nanostructuring. *Nano Res* 2013; 6: 429-40. <https://doi.org/10.1007/s12274-013-0320-z>
- [28] Hwangbo S, Heo J, Lin X, Choi M, Hong J. Transparent superwetting nanofilms with enhanced durability at model physiological condition. *Sci Rep* 2016; 6: 19178. <https://doi.org/10.1038/srep19178>
- [29] Ebert D, Bhushan B. Transparent, superhydrophobic, and wear-resistant coatings on glass and polymer substrates using SiO<sub>2</sub>, ZnO, and ITO nanoparticles. *Langmuir* 2012; 28: 11391-9. <https://doi.org/10.1021/la301479c>
- [30] Li F, Du M, Zheng Q. Transparent and durable SiO<sub>2</sub>-containing superhydrophobic coatings on glass. *J Appl Polym Sci* 2015; 132: n/a – n/a.
- [31] Ahangarani S, Lari N, Shanaghi A. A novel route to prepare hydrophobic and durable antireflective hybrid silica coating by sol-gel method. *Prot Met Phys Chem Surfaces* 2016; 52: 475-80. <https://doi.org/10.1134/S2070205116030175>
- [32] Manca M, Cannavale A, De Marco L, Aricò AS, Cingolani R, Gigli G. Durable superhydrophobic and antireflective surfaces by trimethylsilanized silica nanoparticles-based sol-gel processing. *Langmuir* 2009; 25: 6357-62. <https://doi.org/10.1021/la804166t>
- [33] Zeng C, Wang H, Zhou H, Lin T. Self-cleaning, superhydrophobic cotton fabrics with excellent washing durability, solvent resistance and chemical stability prepared from an SU-8 derived surface coating. *RSC Adv* 2015; 5: 61044-50. <https://doi.org/10.1039/C5RA08040A>
- [34] Dong T, Zhou Y, Hu D, *et al.* Free-standing, flexible, multifunctional, and environmentally stable superhydrophobic composite film made of self-assembled organic micro/super-nanostructures through solution process. *J Colloid Interface Sci* 2015; 445: 213-8. <https://doi.org/10.1016/j.jcis.2014.12.072>
- [35] Wang C-F, Tzeng F-S, Chen H-G, Chang C-J. Ultraviolet-durable superhydrophobic zinc oxide-coated mesh films for surface and underwater-oil capture and transportation. *Langmuir* 2012; 28: 10015-9. <https://doi.org/10.1021/la301839a>
- [36] Jung YC, Bhushan B. Mechanically durable carbon nanotube-composite hierarchical structures with superhydrophobicity, self-cleaning, and low-drag. *ACS Nano* 2009; 3: 4155-63. <https://doi.org/10.1021/nn901509r>
- [37] Huovinen E, Takkunen L, Korpela T, Suvanto M, Pakkanen TT, Pakkanen TA. Mechanically robust superhydrophobic polymer surfaces based on protective micropillars. *Langmuir* 2014; 30: 1435-43. <https://doi.org/10.1021/la404248d>
- [38] Felde N, Coriand L, Duparré A, Notni G. Beschichtung für eine Glasoberfläche, Verfahren zu deren Herstellung und Glaselement. Patent Application DE102014112133 A1. 2016 Feb.
- [39] Duparré A, Ferre-Borrull J, Gliech S, Notni G, Steinert J, Bennett JM. Surface characterization techniques for determining the root-mean-square roughness and power spectral densities of optical components. *Appl Opt* 2002; 41: 154. <https://doi.org/10.1364/AO.41.000154>
- [40] Brinker CJ, Frye GC, Hurd AJ, Ashley CS. Fundamentals of sol-gel dip coating. *Thin Solid Films* 1991; 201: 97-108. [https://doi.org/10.1016/0040-6090\(91\)90158-T](https://doi.org/10.1016/0040-6090(91)90158-T)
- [41] Minami T, Katata N, Tadanaga K. Preparation and characterization of super-water-repellent Al<sub>2</sub>O<sub>3</sub> coating films with high transparency. In: Dunn BS, Mackenzie JD, Pope EJA, Schmidt HK, Yamane M, editors. *SPIE* 1997. p. 168-75.
- [42] Flemming M, Coriand L, Duparré A. Ultra-hydrophobicity through stochastic surface roughness. *J Adhes Sci Technol* 2009; 23: 381-400. <https://doi.org/10.1163/156856108X370082>
- [43] Duparré A, Coriand L. Assessment Criteria for Superhydrophobic Surfaces with Stochastic Roughness. In: Mittal KL, editor. *Advances in Contact Angle, Wettability and Adhesion* Hoboken, NJ, USA: John Wiley & Sons, Inc.; 2013; pp. 197-201. <https://doi.org/10.1002/9781118795620.ch11>
- [44] Duparré A, Flemming M, Steinert J, Reihls K. Optical coatings with enhanced roughness for ultrahydrophobic, low-scatter applications. *Appl Opt* 2002; 41: 3294. <https://doi.org/10.1364/AO.41.003294>
- [45] Coriand L, Mitterhuber M, Duparré A, Tünnermann A. Definition of roughness structures for superhydrophobic and hydrophilic optical coatings on glass. *Appl Opt* 2011; 50: C257-63. <https://doi.org/10.1364/AO.50.00C257>
- [46] Sedin DL, Rowlen KL. Influence of tip size on AFM roughness measurements. *Appl Surf Sci* 2001; 182: 40-8. [https://doi.org/10.1016/S0169-4332\(01\)00432-9](https://doi.org/10.1016/S0169-4332(01)00432-9)
- [47] Dziomba T, Koenders L, Wilkening G. Towards a Guideline for SPM Calibration. In: *Nanoscale Calibration Standards and Methods* Wiley-VCH Verlag GmbH & Co. KGaA; 2005; pp. 171-92. <https://doi.org/10.1002/3527606661.ch13>
- [48] Marmur A. Solid-surface characterization by wetting. *Annu Rev Mater Res* 2009; 39: 473-89. <https://doi.org/10.1146/annurev.matsci.38.060407.132425>
- [49] von Finck A, Herfurth T, Schröder S, Duparré A, Sinzinger S. Characterization of optical coatings using a multisource table-top scatterometer. *Appl Opt* 2014; 53: A259-69. <https://doi.org/10.1364/AO.53.00A259>
- [50] Schröder S, von Finck A, Duparré A. Standardization of light scattering measurements. *Adv Opt Technol* 2015; 4: 361-75. <https://doi.org/10.1515/aot-2015-0041>
- [51] Marmur A. Soft contact: measurement and interpretation of contact angles. *Soft Matter* 2006; 2: 12-7. <https://doi.org/10.1039/B514811C>

© 2016 Felde *et al.*; Licensee Lifescience Global.

This is an open access article licensed under the terms of the Creative Commons Attribution Non-Commercial License (<http://creativecommons.org/licenses/by-nc/3.0/>) which permits unrestricted, non-commercial use, distribution and reproduction in any medium, provided the work is properly cited.